Journal of Thermal Analysis and Calorimetry, Vol. 72 (2003) 907–918

COMPUTER AIDED THERMAL ANALYSIS

V. Strezov [1*], *J. A. Lucas* [2] *and L. Strezov* [3]

[1]Newbolds Applied Research, The University of Newcastle, Cnr Frith and Gavey Streets, Mayfield NSW 2304, Australia
[2]Discipline of Chemical Engineering, Faculty of Engineering and Built Environment, The University of Newcastle, University Drive, Callaghan NSW 2308, Australia
[3]Strezov Consulting, 7 Marin Street, Adamstown NSW 2289, Australia

Abstract

Inverse numerical techniques have been applied in a range of different thermal studies in the past. These techniques require measurements of boundary conditions and temperatures at known position within the sample in order to determine thermal properties of the material of interest. Typically, they have been applied to highly specific applications and designs. In the current work the authors have designed a novel instrument in order to measure apparent specific heats of a range of different materials during continuous heating. Measurements of surface heat flux, surface and centre temperatures of the sample were obtained under controlled heating for temperatures of up to 1000°C. Measured data was used to quantify specific and latent heats by employing inverse numerical modelling technique. The instrument was calibrated with calorimetric calibration materials and results were compared with the literature values. The average experimental error was estimated to be approximately 0.9% for the reaction peak temperatures and 1.7% for the latent heats. Detailed experimental and calculation procedures as well as measured results of specific heat and enthalpy for a number of materials are presented here.

Keywords: inverse methods, latent heat, specific heat, thermal analysis

Introduction

Thermal analysis and calorimetry of materials undergoing transformations during heating has been a subject of study for over a century. A vast range of different techniques has been developed since, the background and classifications of which have been extensively reviewed by Höhne *et al.* [1]. Generally, they can be divided in static and dynamic according to the heating conditions under which they operate. All of the available methods for measurements of specific heat necessarily require steady state heating conditions. The measurements are often time consuming with limited resolution of the results. The enthalpy measurements have, however, improved over the years with the differential methods of analysis, differential thermal analysis (DTA) and differential scanning calorimetry (DSC). Both methods simultaneously

* Author for correspondance: E-mail: Vladimir.Strezov@newcastle.edu.au

1388–6150/2003/ $ 20.00
Akadémiai Kiadó, Budapest

heat the sample and a reference inert material comparing differences in their temperatures or compensating differences in the heats. In both cases measurements are continuous under unsteady-state heating conditions. Although much effort has been placed to apply the DTA method for quantitative studies, it remains in many cases limited leaving the DSC method as the only quantitative dynamic calorimetric technique for enthalpy measurements.

In recent years, however, an extensive progress is evident in utilisation of computer technology in solving specific tasks related to either specific heat and enthalpy, or thermal conductivity of the materials of interest [2–7]. In the field of solidification of metals and related processes, inverse numerical methods have been used for estimation of boundary conditions and thermo-physical properties of materials [3, 4]. Dowding *et al.* [5] have applied the inverse solution for estimation of the thermal properties of carbon-carbon composite. These techniques are generally based upon minimisation of the errors between measured and calculated temperatures at given locations in the sample. Numerical solutions of the heat flow equation are used to calculate temperature within the sample, by employing initial guess value for the surface boundary conditions or thermal properties of the material e.g. specific heat. Using such methods, the estimation of the specific heat is conducted continuously under unsteady-state heating conditions. These techniques have been previously applied for highly specific applications and designs. In the current work authors made an effort to apply the inverse methods in design of an instrument for general estimation of apparent specific heats under continuous heating conditions of a range of different materials.

Design of experimental apparatus

Estimation of the thermal properties by applying inverse numerical technique requires controlled heating conditions with known heat flux and boundary temperature conditions of the heated sample. Most suitable heating methods are either with heat flux plates, where the sample is placed between two plates and heated through one side of the plate while recording boundary temperature conditions; or using cylindrical coordinate system as applied in the design shown in Fig. 1. In the experimental equipment used in this work, the sample is placed in a silica glass tube with 13 mm outside diameter and 1.2 mm wall thickness, while assuring insulation of the sample with alumina-silicate ceramics. The ceramics are machined to allow free gas flow through the sample and to lead the thermocouples to their positions. The thermocouples are well positioned on the surface and in the centre of the sample to monitor the boundary temperature conditions. Graphite tube 265 mm long with 27 mm outside and 17 mm inside diameter is positioned centrically to the sample glass tube. In this way the graphite tube becomes heating element for the sample controlling the heating rate with a single thermocouple embedded in a 3 mm deep groove. The groove is covered and packed with graphite powder. Heat flux through the sample can, in this case, be easily controlled and measured as the heating from the graphite to the sample is achieved predominantly through radiation. For this purpose and to ensure uniform emissivity from the graphite to the sample, the outer surface of the silica sample tube is covered with carbon soot produced from combusted acetylene. This pro-

cedure is performed prior to positioning of the graphite heating element. The experimental design in this case allows heating of the sample with known heat flux and known boundary temperature conditions essential for performing the calculation procedure.

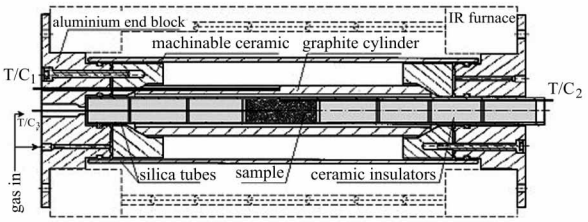

Fig. 1 Cross section of the experimental apparatus. Dashed lines represent infrared image gold furnace SINKU-RIKO. Sample is packed inside a glass silica tube and heated by radiation from the surrounding graphite cylinder. Thermocouples (T/C) are used to monitor temperatures of the graphite, surface and centre of the sample. Heating rate of the furnace is controlled with T/C_1

The furnace used in this work was an infrared gold image furnace model SINKU-RIKO E410. The furnace had maximum power of 8 kW and maximum operating temperature of 1500°C. The heating elements of the furnace are with tubular focusing. Heating zone of the furnace is insulated from the water-cooled sector with machineable alumina-silicate ceramics on sides. Argon gas is continuously flown through the silica sample tube at a rate of 5 mL min^{-1}, removing the volatiles from the furnace and minimising sample oxidation. The graphite tube is also kept under inert conditions with argon flow of 30 mL min^{-1} in the sealed sector of the furnace. The thermocouples used for temperature measurements are type K chromel-alumel thermocouples, 300 mm in length with 1 mm in diameter. Measured temperatures are acquired at a frequency of 1000 Hz, however the logged data is an average of the measurements displayed and stored in the hard disc of the computer each second. In this way, high frequency and resolution of the measurements with low noise in the results is achieved.

Calculation methods

Calculation of the heat flux

The sample is heated from the surrounding graphite cylinder predominantly by radiation. When heat is exchanged between two long concentric cylinders the radiative heat flux can be estimated by:

$$Q = F_{1-2}\,\sigma\,(T_g^4 - T_s^4) \tag{1}$$

where Q is the heat flux (W m^{-2}); F_{1-2} is the radiation shape factor (-); σ is the Stefan-Boltzmann constant (5.67E-8 W m^{-2} K^{-4}) and T_g and T_s are the temperatures of the graphite and the surface of the sample (K), respectively.

The radiation shape factor F_{1-2} is defined as a fraction of diffusely distributed radiation leaving the surface A_1 that reaches the surface A_2 [8]. The radiation shape factor is a function of the emissivities of the two cylindrical surfaces and their surface areas. For concentric cylinders, it is:

$$F_{1-2} = \frac{A_1}{\frac{1}{\varepsilon_1} + \frac{A_1}{A_2}\left(\frac{1}{\varepsilon_2} - 1\right)} \tag{2}$$

where ε_1 and ε_2 are the emissivities of the surfaces A_1 and A_2.

Inverse numerical solution of heat transfer

The one dimensional heat conduction equation is given by:

$$\rho C_p \frac{\partial T}{\partial t} = k \frac{\partial}{\partial r}\left(r \frac{\partial T}{\partial r}\right) \tag{3}$$

where ρ – density (kg m^{-3}), C_p – specific heat (J kg^{-1} K^{-1}), k – thermal conductivity (W m^{-1} K^{-1}), T – temperature (K), t – time (s), r – radius (m).

The specific heat and thermal conductivity are related with the thermal diffusivity α (m^2 s^{-1}), which determines the rate of temperature rise under unsteady-state heating conditions:

$$\alpha = \frac{k}{\rho C_p} \tag{4}$$

where α is thermal diffusivity (m^2 s^{-1}), k is thermal conductivity (W m^{-1}K^{-1}), ρ is density (kg m^{-3}) and C_ρ is specific heat (J m^{-3} K^{-1}).

The fully implicit discretisation equation expressed in radial coordinates for the grid geometry shown in Fig. 2 is presented with Eq. (5), assuming no heat losses in

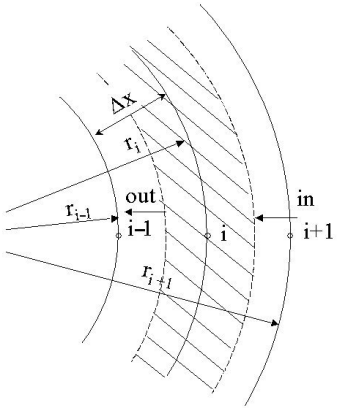

Fig. 2 Sample grid geometry

the sample occurred. The heat balance for each of the node sections is: heat of accumulation = rate of heat in – rate of heat out.

$$\frac{2\pi\Delta x^2 i}{\Delta t\alpha}(T_i^t - T_i^{t-1}) = 2\pi\left(i+\frac{1}{2}\right)(T_{i+1}^t - T_i^t) - 2\pi\left(i-\frac{1}{2}\right)(T_{i-1}^t - T_i^t) \quad (5)$$

Equation (5) was a subject to the surface boundary condition of known temperature and heat flux, and the boundary condition at the centre of the sample of known temperature and zero heat flux.

The product of density and specific heat (volumetric specific heat) is expressed as:

$$\rho C_p = \frac{2\pi n\Delta x Q_{(t)}}{\frac{\Delta x^2\pi}{4\Delta t}(T_0^t - T_0^{t-1}) + \frac{\Delta x^2\pi}{\Delta t}\left(n-\frac{1}{4}\right)(T_n^t - T_n^{t-1}) + \sum_{i=1}^{n-1}\frac{2\pi\Delta x^2 i}{\Delta t}(T_i^t - T_i^{t-1})} \quad (6)$$

where ρC_p is volumetric specific heat (J m^{-3} K^{-1}), n number of nodes (-), T_i^t is the temperature expressed in K of the node i for the time t (s) and $Q_{(t)}$ is the heat flux expressed in W m^{-2} for time t.

Experimental

Calibration procedure

Calculation of the surface heat flux with Eq. (1) requires values for the radiation shape factor F_{1-2}, which is a function of the emmisivities of two bodies transmitting heat between each other and their geometrical configurations. In order to obtain high accuracy in the estimation of the heat flux, radiation shape factor was determined with calibration. Copper sample was chosen as a calibration material as its thermophysical properties have been well defined [9, 10], and it remains stable until 1000°C.

The copper sample was machined to fit inside the glass silica tube and to locate one thermocouple in the centre of the sample. The sample was insulated on both sides with ceramics and the elements of the apparatus were positioned in the furnace as described previously. The copper was heated from room temperature to a maximum of 1000°C at a constant heating rate of 10°C min^{-1}.

The calibration measurements were obtained by monitoring only two temperatures, the temperature of the graphite tube and centre of the copper sample as shown in Fig. 3a. Surface sample temperature and surface heat flux were calculated using inverse numerical solution by applying the measured centre temperature as a boundary condition. The radiation shape factor was finally calculated by applying Eq. (1) and presented in Fig. 3b.

For temperatures of around 200°C and below, the radiation shape factor showed values greater than unity. This was attributed to the contribution of convection on the heat transfer and in further calculations was included as part of the apparent radiation shape factor.

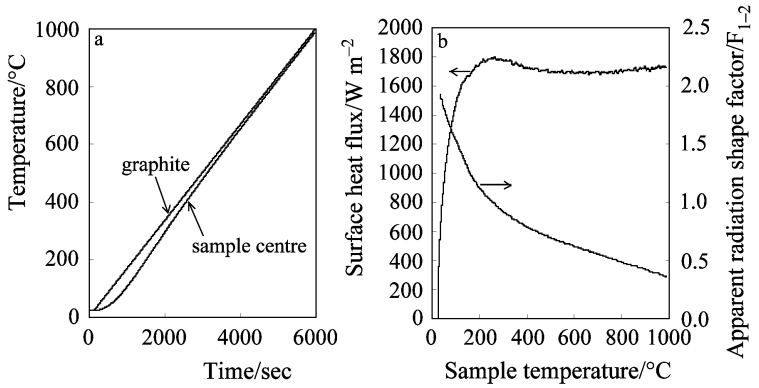

Fig. 3 Calibration results; a – measured graphite and centre sample temperatures; b – calculated sample surface temperature and radiation shape factor

The calibration procedure was repeated several times to test the reproducibility of the calculated surface heat flux. After completion of each experiment, the copper sample was removed from the glass tube. The surface of the copper was cleaned with 10% orthophosphoric acid, and placed in alcohol in an ultrasonic bath for around 20 min. The sample was finally dried and the setting up procedure repeated. Each experiment was performed with new set of thermocouples. The results showed reproducibility with maximum variation of ±8 W m^{-2}.

Features and performance of the equipment

Performance of the equipment was tested on variety of samples to define the accuracy of the measured results. Samples used in the measurements were either solid or a packed bed of powdered material. Solid samples were 30 mm in length machined to fit inside the glass tube and to allow positioning of the thermocouples on the surface and in the centre.

Specific heat

Machined stainless steel sample 253MA was used to measure specific heat and compare with the values available from the supplier of the material. The sample was heated at 10°C min^{-1} until graphite temperature reached 1000°C. The surface heat flux was calculated from the temperature of the graphite and surface of the sample by applying Eq. (1), while the specific heat was calculated numerically. Results are compared in Fig. 4 showing good agreement with an average error of ±0.7%.

Nickel sample was also applied and results compared in Fig. 5a with the well documented values available in the literature. Firstly, the apparent specific heat of nickel was estimated for three consecutive measurements under continuous heating rate of 10°C min^{-1}. This was performed to test the reproducibility of the method on the measured specific heat data. Results from the current method are shown with a solid line. The three measurements overlapped showing reasonably well

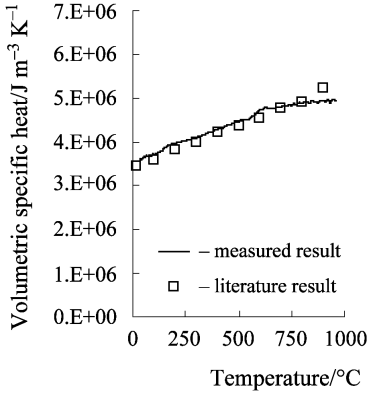

Fig. 4 Comparison between the measured volumetric specific heat of stainless steel 253MA compared with the recommended values from the manufacturer

reproducibility estimated around ±2%. Results represented with various dotted points in Fig. 5a represent values of specific heats of nickel available from fourteen different sources, as found in the literature [9–11]. Most of these results were summarised by Goldsmith *et al.* [10]. Comparisons with the literature data showed very good agreement. It was noticeable that considerable improvement in resolution of the results was achieved with the computational calorimetric method described here. Techniques limited to unsteady-state heating conditions for estimation of specific heats have, in general, limited number of results due to lengthy measurement procedures. They have been usually performed at a large temperature interval showing a single result every 50 to 100°C. The technique shown here provides measurements with continuous heating of the sample at a resolution of 1 Hz, which for the results shown in Fig. 5a, i.e. heating rate of 10°C min^{-1}, is six measurements each °C.

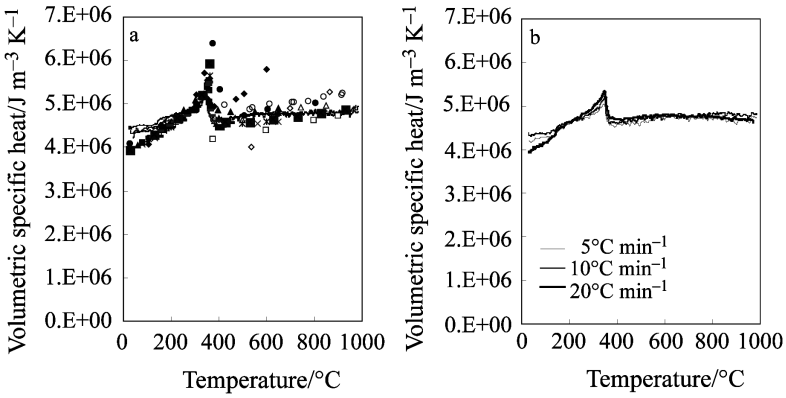

Fig. 5 Experimental results on nickel, a – comparison between three consecutive measurements from the current method with the values reported in the literature [9–11]. Solid lines are results achieved with the current method, while dotted values are reported literature data, b – volumetric specific heat of nickel at three different heating rates 5, 10 and 25°C min^{-1}

A question was raised if the heating rate will affect measurement data. It is known that regardless of the heating rate, specific heat of the material is well defined and remains constant, therefore if any changes occur in the measurements, they would have been due to a measurement error. Solid nickel sample was for this purpose heated at additional two heating rates of 5, and 25°C min^{-1} up to the maximum temperature of 1000°C. Results are compared in Fig. 5b with one of the previous measurements on 10°C min^{-1}. The estimated error for the results shown in Fig. 5b was ±2%. The reproducibility is considered considerably high, showing some deviations at temperatures below 100°C, mainly attributed to the convective heat exchange, which at higher heating rates becomes more effective. With increasing the sample temperatures, however, this effect is negligible.

Heats of transformation

The nickel sample was specifically chosen for testing of the performance of the equipment as it exhibits a distinctive magnetic transformation at 353°C. To calculate the heat of transformation in this work, a straight line baseline was assumed, as shown in Fig. 6a, and the difference between measured specific heat and baseline was integrated. Comparison between the peak temperature and heat of transformation of the current measurements with literature data [10–12] are summarised in Table 1.

Table 1 Comparison of the measured with the literature values for peak temperature and enthalpy

	Sample	Measured		Literature	
		T_{peak}/°C	ΔH/kJ kg^{-1}	T_{peak}/°C	ΔH/kJ kg^{-1}
Transformation	Ni	350	6.78	353	6.56
	K_2SO_4	591	46.8	583	47.3
Melting	Sn	235	60.4	232	60.4
	Pb	323	23.3	327	24.6
Decomposition	$MnCO_3$	452	–	450–600	–
	$Mg(OH)_2$	428	–	400–500	–
	$CaMg(CO_3)_2$	732, 928	–	730, 930	–
Glass transition	Polycarbonate Resin	150	–	149	–
Average error		0.9%	1.7%		

The technique was also tested on powdered potassium sulphate, which has been accepted as a calibration material standard for DSC and DTA [13]. The sample weighting 5.3 g was packed to 2000 kg m^{-3} and heated at 10°C min^{-1}. The estimated apparent volumetric specific heat is shown in Fig. 6b. The endothermic transition ΔH_{tr} was calculated by integrating the difference between the measured apparent spe-

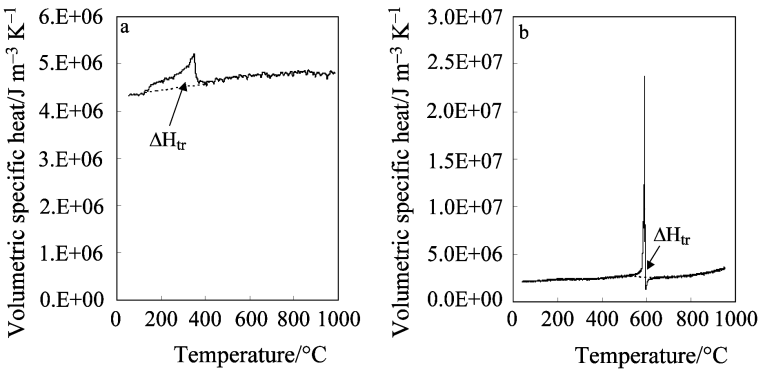

Fig. 6 Thermal curves representing transformation; a – nickel, b – K_2SO_4

cific heat and the baseline, over the temperature range. Comparison of the measured values with published data is shown in Table 1.

Heats of melting

Proposed experimental design is unsuitable for heating of materials in a liquid state as the material tends to leak on the sides towards the ceramic insulators. However, measurement of the heats of melting could be achieved if the sample is mixed with an inert material, which becomes an absorbent when the liquid phase takes place. In this work 1:1 mass ratio of the sample was mixed with alumina and samples heated at a heating rate of 3°C min^{-1}. Two separate measurements of tin and lead, which are also recommended as calorimetric calibration materials, are illustrated in Fig. 7. The apparent specific heat obtained was the specific heat of mixture of sample with alumina. The heat of melting was determined in a procedure identical with the transformations. The packing density was used to convert the units in kg bases and value doubled to obtain the heat of melting of pure material. Results of the peak temperatures and heats

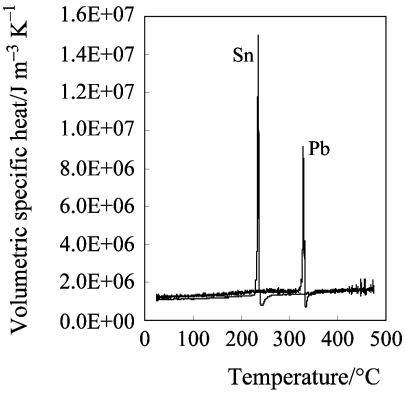

Fig. 7 Specific heat of 1:1 mixture of tin/lead with alumina. Peaks represent melting point of the material

of melting are compared with literature values [1, 13] in Table 1. Again, well agreement was achieved from the current method with the published data.

Thermal decomposition

When thermal decomposition occurs and volatiles are being generated, the positive gas carrier pressure ensures volatiles are being released outside the furnace and could be further taken to a gas detector and analyser. Depending on the mass loss the sample volume could change significantly affecting the quantitative accuracy of the measured data. Therefore, the method of mixtures with an inert material could be applied to ensure constant volume of the sample throughout the heating. Three samples were analysed for the purpose of this study and results are illustrated in Fig. 8. The reaction peak temperatures are compared with literature data [14] in Table 1. The chosen materials are not suitable for calorimetric enthalpy calibration as the heat of decomposition and peak temperatures of these samples are heavily dependent on their purity and origin. For manganese carbonate and magnesium hydroxide there is a wide temperature range where the peak temperature could occur. However, the decomposition peaks are distinctive forming metallic oxides and evolving carbon dioxide in both cases. The dual peak in dolomite thermal curve (Fig. 8c) is due to the two-stage decomposition process where the first peak represents decomposition of magnesium carbonate, while the second peak is due to decomposition of calcium carbonate.

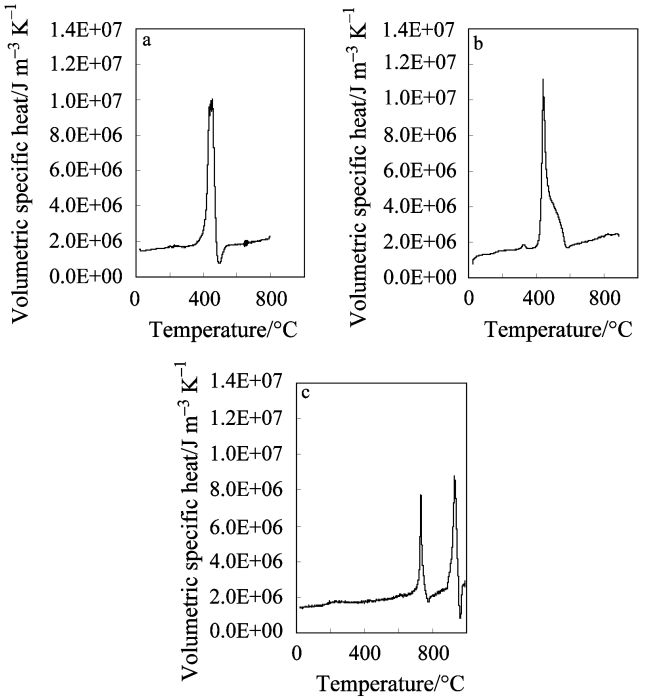

Fig. 8 Thermal curves of selected samples; a – $MnCO_3$, b – $Mg(OH)_2$ and c – $CaMg(CO_3)_2$

Glass Transition

Glass transitions are commonly encountered in polymers. The glass transition represents an increase in the specific heat due to the structural relaxation of the amorphous chain segments. A polycarbonate resin supplied from Sigma Aldrich was heated at 10°C min^{-1} in this work and the result is shown in Fig. 9. A distinguished shift in the specific heat appeared at 150°C representing the glass transition. The peak corresponds well with the 149°C recommended by the manufacturer. It is noticeable that increase in the specific heat is somewhat small, at least comparing to the changes in specific heats shown in previous figures. This is mainly due to the origin of the transition and it certainly has differences in the changes in the energy state from those of melting or decomposition. Glass transition is a change of state where below the glass transition temperature, the polymer motions are limited, while above the glass transition, intermolecular motions follow a glass route.

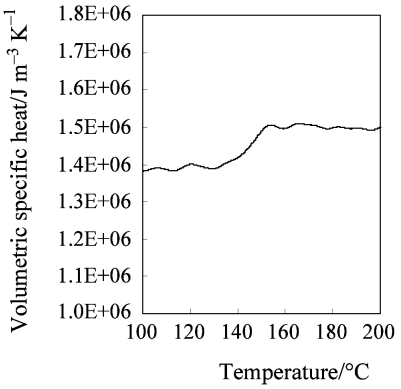

Fig. 9 Glass transition of polycarbonate resin

Conclusions

A novel instrument was designed by the authors to perform thermal analysis during continuous heating. Proposed design is only a possible option the computer aided thermal analysis could further develop. In this case the infrared image furnace was chosen for its fast heating and cooling rate capabilities. The instrument measures the surface heat flux and the boundary temperature conditions on the surface and centre of the sample. The inverse numerical technique was applied to calculate the apparent specific heat at a frequency of 1 Hz. The technique was tested on a number of calorimetric standards and compared with the recommended values for the peak temperatures and enthalpies. The average error of 0.9% for the peak temperature and 1.7% for the enthalpy was obtained. The method has an advantage of significantly high resolution of the results, continuous measurements of the specific heat under unsteady-state heating conditions and capability of detecting small enthalpy changes with high accuracy. A vast range of different heating rates could be applied which are limited only with the performance capabilities of the equipment. However, the specific heat determined with the current method is volumetric

and conversion based on the original sample mass could be calculated including the packing density. If sample melting is expected the measurements should be taken with care. The sample, in such conditions, could be mixed with an inert material to retain the desired volume throughout the heating.

* * *

The support of the research was provided by the Australian Research Council.

References

1 G. W. H. Höhne, W. Hemminger and H.-J. Flammersheim, Differential Scanning Calorimeter. An Introduction for Practitioners, Springer-Verlag, Berlin 1996.
2 V. Strezov, J. A. Lucas and L. Strezov, Metal. Mater. Trans. B, 31B (2000) 1125.
3 J. V. Beck, B. Blackwell and C. R. St Clair, Inverse Heat Conduction – Ill Posed Problems, John Wiley, New York 1985.
4 L. Strezov and J. Herbertson, ISIJ Int., 38 (1998) 959.
5 K. J. Dowding and B. F. Blackwell, Meas. Sci. Technol., 9 (1998) 877.
6 K. J. Dowding, J. V. Beck and B. F. Blackwell, J. Thermophys. Heat Transfer, 13 (1999) 328.
7 F. Kowsary and M. Ahmadi, Eur. Congr. on Comp. Methods in Appl. Sci. and Eng. ECCOMAS 11–14 Sept. 2000 Barcelona.
8 F. Kreith and M. S. Bohn, 'Principles of Heat Transfer', Harper and Row Publ., 1986.
9 R. H. Perry and C. H. Chilton, 'Perry's Chemical Engineers' Handbook', Fifth edition, McGraw-Hill International Editors, 1973.
10 A. Goldsmith, T. E. Waterman and H. J. Hirchborn, 'Handbook of Thermophysical Properties of Solid Materials', Vol. 1, The Macmillan Co., 1961.
11 E. O. Schmidt and W. Leidenfrost, Int. J. Heat Mass Transfer, (1962) 267.
12 R. C. Weast 'CRC Handbook of Chemistry and Physics', CRC Press Inc., D-63, 1981.
13 A. Blazek, 'Thermal Analysis', Van Nostrand Reinhold Co., London 1973, p. 165.
14 D. N. Todor, 'Thermal Analysis of Minerals', Abacus Press, Tunbridge West 1976.